PROPOSAL FOR A MECHANICAL MODEL OF MOBILE SHALES

Juan Soto (juan.soto@beg.utexas.edu)
The University of Texas at Austin https://orcid.org/0000-0001-5428-5329
Mahdi Heidari
The University of Texas at Austin
Michael Hudec
University of Texas at Austin

Article

Keywords:

Posted Date: May 19th, 2021

DOI: https://doi.org/10.21203/rs.3.rs-537378/v1

PROPOSAL FOR A MECHANICAL MODEL OF MOBILE SHALES

Juan I. Soto[1,2] [*], Mahdi Heidari[1], and Michael R. Hudec[1]

(1) Bureau of Economic Geology, Jackson School of Geosciences, The University of Texas at Austin, University Station, Box X, Austin, Texas, 78713-8924, USA

(2) On leave of absence from: Departamento de Geodinámica, Universidad de Granada, Avenida de Fuente Nueva s/n, 18071 Granada, Spain

(*) Corresponding author: juan.soto@beg.utexas.edu

Structural systems involving mobile shale represent one of the most difficult challenges for geoscientists dedicated to exploring the subsurface structure of continental margins. Mobile-shale structures range from surficial mud volcanoes to deeply buried shale diapirs and shale-cored folds. Where mobile shales occur, seismic imaging is typically poor, drilling is hazardous, and established principles to guide interpretation are few. The central problem leading to these issues is the poor understanding of the mechanical behaviour of mobile shales. Here we propose that mobile shales are at critical state, and discuss how this proposition can explain key observations associated with mobile shales. The critical-state model can explain the occurrence of both fluidized shales (e.g., in mud volcanoes) and more viscous shales flowing with grain-to-grain contact (e.g., in mud diapirs), mobilization of cemented or compacted materials, and the role of overpressure in shale mobility. Our model offers new avenues for understanding complex and fascinating mobile-shale structures.

Mobile shales are bodies of highly sheared shale that lack coherent reflections in seismic images. Mobile-shale structures range from surficial mud volcanoes to deeply buried shale diapirs and shale-cored folds (Fig. 1a–e). Although they exist in all tectonic regimes (Fig. 1f), they are mostly found in shortening settings (40%) or delta systems on continental margins (31%) (detailed information in Supplementary Discussion 1).

Mobile shales create challenges for seismic processing, seismic interpretation, drilling, and geohazards analysis. A primary source of uncertainty in interpreting these structures is a poor understanding of the mechanics of mobile shale. Although mobile shales appear to deform through some sort of ductile flow[1–3], we have little insight into what can make shales flow. Most authors suggest that shales become mobile simply by becoming highly overpressured[4–5], although this simple model fails to account for the full range of mobile-shale occurrence. For example, shales (defined broadly, *sensu* Aplin et al.[6]) can apparently become mobile even after significant burial, consolidation, and cementation[7–8]. Overpressure can mobilize unconsolidated mud, but an increase in pore pressure alone cannot cause a cemented shale to flow.

Our lack of a viable mechanical model for mobile shale is due partly to the difficulty in sampling subsurface mobile shales. Although mud volcanoes have been extensively studied[9–13], little progress has been made in studying plastic flow of mobile shales using sampling observations[2,14–17] or drilling data[18–19]. As a result, we have little knowledge of the physical properties of plastically flowing shales in the subsurface and even less knowledge of the mechanical processes by which they become mobile or stop moving.

This uncertain understanding is reflected in the existing definition of *mobile shale*. The term was introduced by Morley and Guerin[1], who defined them as “any shales deforming complexly by a

35 combination of ductile deformation and brittle failure in the presence of a fluid phase." This
36 definition was an excellent starting point because it recognized the roles of lithology,
37 deformation style, and fluids in shale mobility. However, it suffers from several shortcomings.
38 First, the definition is overly broad because it includes almost any type of deformation involving
39 shales. Second, it provides little insight into what makes a mobile shale mobile or how it
40 deforms.

41 In this paper, we summarize observations concerning mobile shales, and then propose a
42 mechanical model that can explain these observations. We explore the implications of this model
43 and its answers to key questions in mobile-shale research: How do shales become mobile? Is
44 deformation in mobile shales brittle, ductile, or both? Why do some mobile shales become
45 immobile? Can shales with diagenetic cements become mobile? Does depth of burial play a role
46 in shale mobilization? Do all mobile shales have to be highly overpressured? If so, how high
47 must the overpressure be? How does shale mobilization affect its seismic properties?

48

49 What do we know about the mechanics of mobile shales?

50 There are some observations about mobile shales that are widely accepted. We use these
51 observations as a framework to suggest a mechanical model for mobile shales.

52 First, there are two distinct types of mobile-shale structures[3]. The first occurs when the shale
53 behaves as a fluid suspension without grain-to-grain contact[20-21]. Because of their low viscosity,
54 this type of mobile shales forms smaller features like mud volcanoes (Fig. 1a–b) in which the
55 shale moves at high velocities (up to tens of meters per second)[11–13,22]. In the second type, shale
56 behaves as a viscous-plastic solid involving grain-to-grain frictional flow[2] or creep[23]. Because of

57 their high viscosity, this type of mobile shale forms large-scale bodies like shale diapirs (Fig.
58 1c–e) that move at lower velocity than in mud volcanoes.

59 Second, bedding and other fabrics in mobile-shale structures are strongly disrupted, recording
60 large and extensive shear deformation. This disruption is one factor causing the loss of seismic
61 signal in mobile shale (Fig. 1c–e)[24,25].

62 Third, mobile shales are typically associated with high overpressures. Overpressure is obvious in
63 the fluidized material erupted from mud volcanoes, where there is almost no contact between
64 grains[9,10,11,13,14]. High overpressure in other types of mobile shales such as shale diapirs can be
65 inferred from the low seismic velocities of these bodies[1,3,18,24,26]. Most researchers attribute these
66 overpressures to a combination of increase in the volume of the pore fluid (due to, e.g.,
67 hydrocarbon generation and cracking, diagenetic transformations, or thermal expansion) and in
68 total compressive stresses[27]. For example, based on the abundance of methane expelled during
69 mud-volcano eruptions[9-14,22], the mobility of shale in mud volcanoes is attributed to hydrocarbon
70 transformations and the depressurization of a gas-charged source layer.

71 Fourth, given the stratigraphic position of blocks ejected from mud volcanoes, some mobile
72 shales are sourced from depths of 9 to 10 km[11,13,22,28–30] (detailed information in Supplementary
73 Discussion 1). Units sourced from these depths were cemented prior to incorporation in mud
74 volcanoes. This observation represents a challenge for workers in mobile shales, because it is
75 difficult to explain how these cemented blocks were mobilized.

76 Any viable mechanical model for mobile shales must be able to explain and be consistent with
77 these observations: fluidization and plastic flow of shales, disruption of fabrics, existence of high
78 overpressure, and mobilization of cemented units.

Mechanical model for mobile shales: deformation at the critical state

As mentioned earlier, field observations of subsurface mobile shales are scarce owing to the understandable reluctance of drillers to penetrate them. We therefore turn to experimental deformation of shales, to examine whether they provide any explanation for mobile-shale behaviour. Because these tests are typically conducted at low stresses and on poorly lithified soils, they do not directly mimic subsurface conditions. The principles governing the mechanical behaviour of soils[31–32] have also been used to analysed the behaviour of consolidated shales, although important differences exist between the mechanical behaviour of soils and shales[33–35]. According to these studies, shales differ from soils in that they have a major cohesion (stiffness), develop some degree of cementation and anisotropy, and their mechanical characteristics change with depth and temperature (detailed information in Supplementary Discussion 2, Table s2 and Fig. s4). Principles of soil mechanics have also begun to be extrapolated to depths at which diagenetic transformations operate in shales so that the mechanical behaviour of cemented shales deformed under contraction might be modeled[36–38].

We use the behaviour observed in laboratory tests to infer the mechanical behaviour of mobile shales. Figure 2 illustrates the stress paths and the stress-strain response obtained from undrained triaxial tests on Norrköping clays[39] (Fig. 2). In these tests, the clay sample, retrieved from a core, was first consolidated under uniaxial-strain condition to the in situ vertical effective stress (point B, Fig. 2). This represents the loading on the clay as it was buried to its final depth. Then, the sample was compressed horizontally in undrained conditions; during this period, the total vertical stress was kept constant (path BCD, Fig. 2). This represents the loading that the clay

would undergo if it was in a shortening region, a common setting for mobile shales (Fig. 1f). The test was conducted under undrained conditions because shales have very low permeability, therefore, pore fluid could barely drain out of buried shales during shortening.

The clay response during undrained shortening includes two distinct phases (path BCD, Fig. 2b). First is a period of strain hardening (BC), during which deviatoric stress (q, ordinate axis in Fig. 2a) increases as the clay is compressed horizontally and the shear deformation increases. During this period, the effective mean stress (p′, abscissa axis in Fig. 2a) decreases. The sample tends to compact as it is sheared, but this compaction is prevented by pore fluid that cannot escape, leading to an increase in pore pressure (shear-induced overpressure) and decrease in effective mean stress. The strain-hardening phase occurs at relatively low strains (point C in Fig. 2b).

The second stage consists of strain-weakening behaviour (CD, Fig. 2b), during which deviatoric stress (q) decreases. Softening is attributed to the collapse of rock fabric or breakage of cementation/bonds, also known as *destructuration*[40] (sketches in Fig. 2). Destructuration entails elevated rock compression, which, in undrained conditions, translates into a significant increase in pore pressure (u_D, Fig. 2a) and decrease in effective mean stress[32,41].

The clay reaches a state where stresses almost stop changing (point D, Fig. 2), even though the sample is still being shortened and deformed. This is the critical state, at which unlimited (plastic) shear deformation occurs without any changes in stresses or volume[31,42-43] (plateau, Fig. 2b). The material in fact flows at the critical state, destroying the material fabric or cement (schematic boxes, Fig. 2).

Vane tests show that the clay flow at critical state is viscous, that is, the strain rate at critical state varies with shear stress (Fig. s6 in Supplementary Discussion 2). As such, the clay behaves as a Herschel-Bulkley material: it is solid (no flow) when shear stress is smaller than the static shear

strength, and when shear stress exceeds the strength, it flows at a strain rate that increases with the excess shear stress.

Destructuration of fabric, breaking of cement, large shear deformation, high overpressure, and plastic flow associated with the critical state tie this state to mobile shales. We therefore propose that mobile shales are at the critical state and suggest the following definition for mobile shales: "bodies of clay-rich sediment or sedimentary rock undergoing penetrative, (visco-) plastic deformation at the critical state."

Implications of a critical-state model for mobile shales

Fluidized behaviour vs grain-to-grain plasticity

The critical-state model can explain not only the viscous-plastic behaviour of shales in structures such as shale diapirs, but also the fluid-like behaviour of fluidized shales in mud volcanoes. At critical state, all cements and bonds are destroyed, and the material flow is purely frictional (failure envelope has no cohesion and passes through the origin in a $p'-q$ diagram). Thus, when pore pressure increases in mud volcanoes so much as to bring the effective stresses to zero, the grains lose contact, and the shear strength becomes zero (Figs. 2a and s2 in Supplementary Discussion 2). In this case, the Herschel-Bulkley behaviour converges to a viscous-fluid model, which corresponds to the behaviour of the fluidized shale in mud volcanoes (further details in Supplementary Discussion 2 and Fig. s6).

The drop in effective stress leading to fluidization of shales in mud volcanoes may result from a combination of an increase in fluid pressure and a drop in total stress. One important scenario producing fluidization occurs when mobile shales rise up a fracture system below a mud

146 volcano. Total stress decreases as the material approaches the surface. This drop in total stress
147 during rise leads to methane exsolution, elevating the pore pressure. This combination can bring
148 effective stresses to zero, leading to the highly fluidized *ejecta* sourced from mud volcanoes.

149 *Brittle vs. ductile behaviour*

150 There is a longstanding debate concerning the relative importance of brittle and ductile
151 behaviour in mobile shales[1–3,44]. Brittle behaviour is seen in a stress-strain plot with a strain-
152 softening behaviour; i.e., residual strength at the critical state is significantly lower than peak
153 strength (Figs. 2a–3a). Conversely, ductile behaviour exhibits strain hardening, having similar
154 residual and peak strengths (Fig. 3). The critical-state model suggests that shales with either
155 behaviour can reach the critical state (plateau at the end of the curves) and become mobile (Fig.
156 3a). In Figure 2, for example, the sample reaches the critical state through brittle behaviour. A
157 shale can behave in a brittle or ductile way, depending in part on confining stress and
158 temperature[45–47] (Figs. 3a–b and s3–s4 in Supplementary Discussion 2).

159 Although deformation is ductile once the critical state is reached, any brittle structures formed
160 during approach to the critical state may be preserved during critical-state flow to present a
161 mixture of structural styles.

162 *Pore-fluid pressure*

163 Low velocity of mobile shales suggests overpressure is high in these shales[1,3–5,8,18–19,24–29]. The
164 critical-state-model provides insight into the role that overpressure plays in shale mobilization. In
165 principle, it is possible to reach the critical state (see the critical state line in the p′–q diagram in
166 Fig. 2a) purely through an increase in shear, without any increase in pore pressure. However,
167 increase in pore pressure decreases effective confining (mean) stress, making it possible to reach

168 critical state at lower shear stress. Without high overpressure, forces driving shear stress in
169 mobile shales may not be enough to bring the shales to critical state and make them mobile. This
170 explains the observed link between shale mobility and high pore pressures.

171 Several sources have been suggested to increase pore pressure in mobile shales, including
172 disequilibrium compaction or generation of hydrocarbons[27]. The critical state model suggests
173 shear-induced overpressure as another mechanism for increasing pore pressure in mobile shales
174 during deformation (cf. blue curve in Fig. 2b, and Figs. s2–s4 in Supplementary Discussion 2).

175 *Degree of consolidation*

176 The critical-state concept can explain mobilization of both granular and consolidated
177 material[33–38]. Consolidated or cemented shales have a higher shear strength than unconsolidated
178 materials, particularly when they are compressed parallel to the fabric or stratification (Figs. 3c
179 and s5 in Supplementary Discussion 2). It thus takes higher shear stress to break cements and
180 drive these shales to the critical state. However, once this disaggregation occurs, critical-state
181 flow can occur just as in any other shale.

182 In contrast to previous interpretations[8], critical-state mechanics thus suggests that there is no
183 depth or temperature limit on the formation of mobile shales (Figs. 3 and s2–s4 in
184 Supplementary Discussion 2), Even if cementation has occurred, mobilization in deep shales
185 remains possible—it just takes a higher shear stress to overcome their strength.

186 *End of shale mobility*

187 In many areas, stratal patterns on seismic data suggest that some formerly mobile shales became
188 later inactive (Figs. 1c–e). The critical-state model provides an explanation for stabilization of
189 formerly mobile shales. According to our model, mobile shales stop deforming when the shear

stress becomes smaller that the static shear strength (Fig. s6 in Supplementary Discussion 2). This may occur through either a drop in shear stress or an increase in shear strength, because in either case the shale would depart from critical-state conditions (Figs. 2–3). For example, in shales that have become mobile due to regional shortening, shear stresses may drop if shortening stops. Shear strength might increase due to dissipation of overpressure, which increases the effective mean stress and thereby the shear strength.

Seismic properties

The critical-state model also gives insight into seismic properties of mobile shales. First, it predicts that overpressure increases in mobile shales due to shear deformation (Figs. 2b and s2–s4 in Supplementary Discussion 2) and seismic velocity thus decreases, which affect the seismic impedance of the shales. Second, shear stiffness of a material drops significantly approaching the critical state. Therefore, our model predicts that mobile shales should have a lower S-wave velocity than immobile shales at the same porosity[18–19,48]. Third, although flow at the critical state destroys preexisting rock fabrics, it may create new flow fabrics[2]. Seismic anisotropy is therefore affected.

An important consideration in seismic imaging of mobile shales is whether the shales are presently mobile—that is, whether they are presently at the critical state. Once shales leave the critical state, overpressures and shale stiffness may return to normal values. However, any changes in anisotropy will remain.

In conclusion, we suggest that the critical-state model is a viable hypothesis for the mechanical behaviour of mobile shales. It explains the key observations related to mobile shales, and offers many exciting prospects for future research. We look forward to seeing tests of this hypothesis as the study of mobile shales advances into the future.

References

1. Morley, C. K. & Guerin, G. Comparison of gravity-driven deformation styles and behavior associated with mobile shales and salt. *Tectonics* **15**, 1154-1170 (1996).
2. Morley, C. K., von Hagke, C., Hansberry, R. L., Collins, A. S., Kanitpanyacharoen, W. & King, R. Review of major shale-dominated detachment and thrust characteristics in the diagenetic zone: Part I, meso- and macroscopic scale. *Earth Sci. Rev.* **173**, 168-228 (2017).
3. Wood, L. in *Shale Tectonics* (ed. Wood, L.) 1-4 (*AAPG Mem.* **93**, 2010).
4. Morley, C. K., Tingay, M., Hillis, R. & King, R. Relationship between structural style, overpressures, and modern stress, Baram Delta Province, northwest Borneo. *J. Geophys. Res.* **113**, B09410 (2008).
5. Duerto, L. & McClay, K. Role of the shale tectonics on the evolution of the Eastern Venezuelan Cenozoic thrust and fold belt. *Mar Pet. Geol.* **28**, 81-108 (2011).
6. Aplin, A. C., Fleet, A. J. & Macquaker, J. H. S. in *Muds and Mudstones: Physical and Fluid Flow Properties* (eds. Aplin, A. C., et al.) 1-8 (*Geol. Soc. Spec. Publ.* **158**, 1999).
7. Peltonen, C., Marcussen, Ø., Bjørlykke, K. & Jahren, J. Clay mineral diagenesis and quartz cementation in mudstones: the effects of smectite to illite reaction on rock properties. *Mar. Pet. Geol.* **26**, 887-898 (2009).
8. Day-Stirrat, R. J., McDonnell, A. & Wood, L. J. in *Shale Tectonics* (ed. Wood, L.) 5-27 (*AAPG Mem.* **93**, 2010).
9. Milkov, A. V. Worldwide distribution of submarine mud volcanoes and associated gas hydrates. *Mar. Geol.* **167**, 29-42 (2000).
10. Dimitrov, L. I. Mud volcanoes—the most important pathway for degassing deeply buried sediments. *Earth Sci. Rev.* **59**, 49-76 (2002).
11. Kopf, A. Significance of mud volcanism. *Rev. Geophys.* **40**, 1005 (2002).
12. Alizadeh, A. A., Guliev, I. S., Dadashov, F. H. & Rahmanov, R. R. *Atlas of the World Mud Volcanoes* (Nafta-Press, Baku, 2015).
13. Mazzini, A. & Etiope, G. Mud volcanism: An updated review. *Earth Sci. Rev.* **168**, 81-112 (2017).
14. Kerr, P. F., Drew, I. M. & Richardson, D. S. Mud volcano clay, Trinidad, West Indies. *AAPG Bull.* **54**, 2101-2110 (1970).
15. Williams, P. R., Piagram, C. J. & Dow, D. B. Melange production and the importance of shale diapirism in accretionary terrains. *Nature* **309**, 145-146 (1984).
16. Petley, D. N. in *Muds and Mudstones: Physical and Fluid Flow Properties* (eds. Aplin, A. C., et al.) 61-71 (*Geol. Soc. Spec. Publ.* **158**, 1999).
17. Kopf, A. J., Clennell, B. & Brown, K. M. in *Mud Volcanoes, Geodynamics and Seismicity* (eds. Martinelli, G. & Panahi, B.) 263-283 (Springer, 2005).
18. Henry, M., Pentilla, M. & Hoyer, D. in *Shale Tectonics* (ed. Wood, L.) 63-78 (*AAPG Mem.* **93**, 2010).
19. Lupi, M., Saenger, E. H., Fuchs, F. & Miller, S. A., 2013. Lusi mud eruption triggered by geometric focusing of seismic waves. *Nat. Geosci.* **6**, 642-688 (2013).
20. Pralle, N., Külzer, M. & Gudehus, G. in Subsurface Sediment Mobilization (eds. Van Rensbergen, P., et al.) 159-171 (*Geol. Soc. Spec. Publ.* **216**, 2003).
21. Tran, A., Rudolph, M. L. & Manga, M. Bubble mobility in mud and magmatic volcanoes. *J. Volcanol. Geotherm. Res.* **294**, 11–24 (2015).
22. Mazzini, A. et al. Explosive mud volcano eruptions and rafting of mud breccia blocks. *Earth Planet. Sci. Lett.* **555**, 116699 (2021).
23. Haghighat, E., Rassouli, F. S., Zoback, M. D. & Juanes, R. A viscoplastic model of creep in shale. *Geophys.* **85**, MR155-MR166 (2020).
24. Roberts, K. S., Davies, R. J. & Stewart, S. A. Structure of exhumed mud volcano feeder complexes, Azerbaijan. *Basin Res.* **22**, 439–451 (2010).
25. Soto, J. I., Fernández-Ibáñez, F., Talukder, A. R. & Martínez-García, P. in *Shale Tectonics* (ed. Wood, L.) 119-144 (*AAPG Mem.* **93**, 2010).
26. Soto, J. I., Hudec, M. R., Mondol, N. H. & Heidari, M. Shale transformations and physical properties—implications for seismic expression of mobile shales. *Earth Sci. Rev.* (under review).
27. Osborne, M. J. & Swarbrick, R. E. Mechanisms for generating overpressure in sedimentary basins: A reevaluation. *AAPG Bull.* **81**, 1023-1041 (1997).
28. Inan, S. et al. Deep petroleum occurrences in the Lower Kura Depression, South Caspian Basin, Azerbaijan: an organic geochemical and basin modelling study. *Mar. Pet. Geol.* **14**, 731-762 (1997).

29. Planke, S. et al. Mud and fluid migration in active mud volcanoes in Azerbaijan. *Geo-Mar. Lett.* **23**, 258-268 (2003).
30. Sautkin, A. et al. Mud volcanoes in the Alboran Sea: evidence from micropaleontological and geophysical data. *Mar. Geol.* **195**, 237-261 (2003).
31. Roscoe, K. H. & Burland, J. B. in *Engineering Plasticity* (eds. Heyman, J. & Leckie, F. A.) 535-609 (Cambridge University Press, Cambridge, 1968).
32. Schofield, A. N. & Wroth, C. P. *Critical State Soil Mechanics* (McGraw-Hill, London, 1968).
33. Steiger, R. P. & Leung, P. K. Quantitative determination of the mechanical properties of shale. *SPE Drill. Complet.* **7**, 181-185 (1992).
34. Horsrud, P., Sønstebø, E. F. & Bøe, R. Mechanical and petrophysical properties of North Sea shales. *Int. J. Rock Mech. Min. Sci.* **35**, 1009-1020 (1998).
35. Ewy, R., Dirkzwager, J. & Bovberg, C. Claystone porosity and mechanical behavior vs. geologic burial stress. *Mar. Pet. Geol.* **121**, 104563 (2020).
36. Albertz, M. & Sanz, P. F. Critical state finite element models of contractional fault-related folding: Part 2. Mechanical analysis. *Tectonophysics* **576-577**, 150-170 (2012).
37. Obradors-Prats, J., Rouainia, M., Aplin, A. C. & Crook, A. J. L. Hydro-mechanical modelling of stress, pore pressure and porosity evolution in fold-and-thrust belt systems. *J. Geophys. Res. B: Solid Earth* **122**, 9383-9403 (2017).
38. Obradors-Prats, J., Rouainia, M., Aplin, A. C. & Crook, A. J. L. A diagenesis model for geomechanical simulations: formulation and implications for pore pressure and development of geological structures. *J. Geophys. Res. B: Solid Earth* **124**, 4452-4472 (2019).
39. Westerberg, B. *Lerors Mekaniska Egenskaper: Experimentell Bestämning och Kvalitativ Modellering med Tillämpning på Lera från Norrköping* [Licenciate thesis, Luleå University of Technology, Sweden] (1995).
40. Rouainia, M. & Muir Wood, D. A kinematic hardening constitutive model for natural clays with loss of structure. *Géotechnique* **50**, 153-164 (2000).
41. Lambe, T. W. & Whitman, R. V. *Soil Mechanics* (SI Version, 2nd ed) (John Wiley & Sons, New York, 1979).
42. Atkinson, J. H. & Bransby, P. L. *The Mechanics of Soils: An Introduction to Critical State Soil Mechanics* (McGraw-Hill, London, 1978).
43. Muir Wood, D. *Soil Behaviour and Critical State Soil Mechanics* (Cambridge University Press, Cambridge, 1991).
44. Restrepo-Pace, P. A. in *Passive Margins: Tectonics, Sedimentation and Magmatism* (ed. McClay, K. R. & Hammerstein, J. A.) 193-204 (*Geol. Soc. Spec. Publ.* **476**, 2020).
45. Rybacki, E., Meier, T. & Dresen, G. What controls the mechanical properties of shale rocks? – Part II: Brittleness. *J. Pet. Sci. Eng.* **144**, 39-58 (2016).
46. Wang, S. et al. A universal method for quantitatively evaluating rock brittle-ductile transition behaviors. *J. Pet. Sci. Technol.* **195**, 107774 (2020).
47. Masri, M., Sibai, M., Shao, J. F. & Mainguy, M. Experimental investigation of the effect of temperature on the mechanical behavior of Tournemire shale. *Int. J. Rock Mech. Min. Sci.* **70**, 185-191 (2014).
48. Couzens-Schultz, B. A. & Azbel, K. Predicting pore pressure in active fold−thrust systems: An empirical model for the deepwater Sabah foldbelt. *J. Struct. Geol.* **69**, 465-480 (2014).
49. Hovland, M., Imbert, P. & Ho, S. Fluid venting system website. https://www.fluid-venting-system.org (accessed in June 2020).
50. Islam, M. A. & Skalle, P. An experimental investigation of shale mechanical properties through drained and undrained test mechanisms. *Rock Mech. Rock Eng.* **46**, 1391-1413 (2013).

Figures

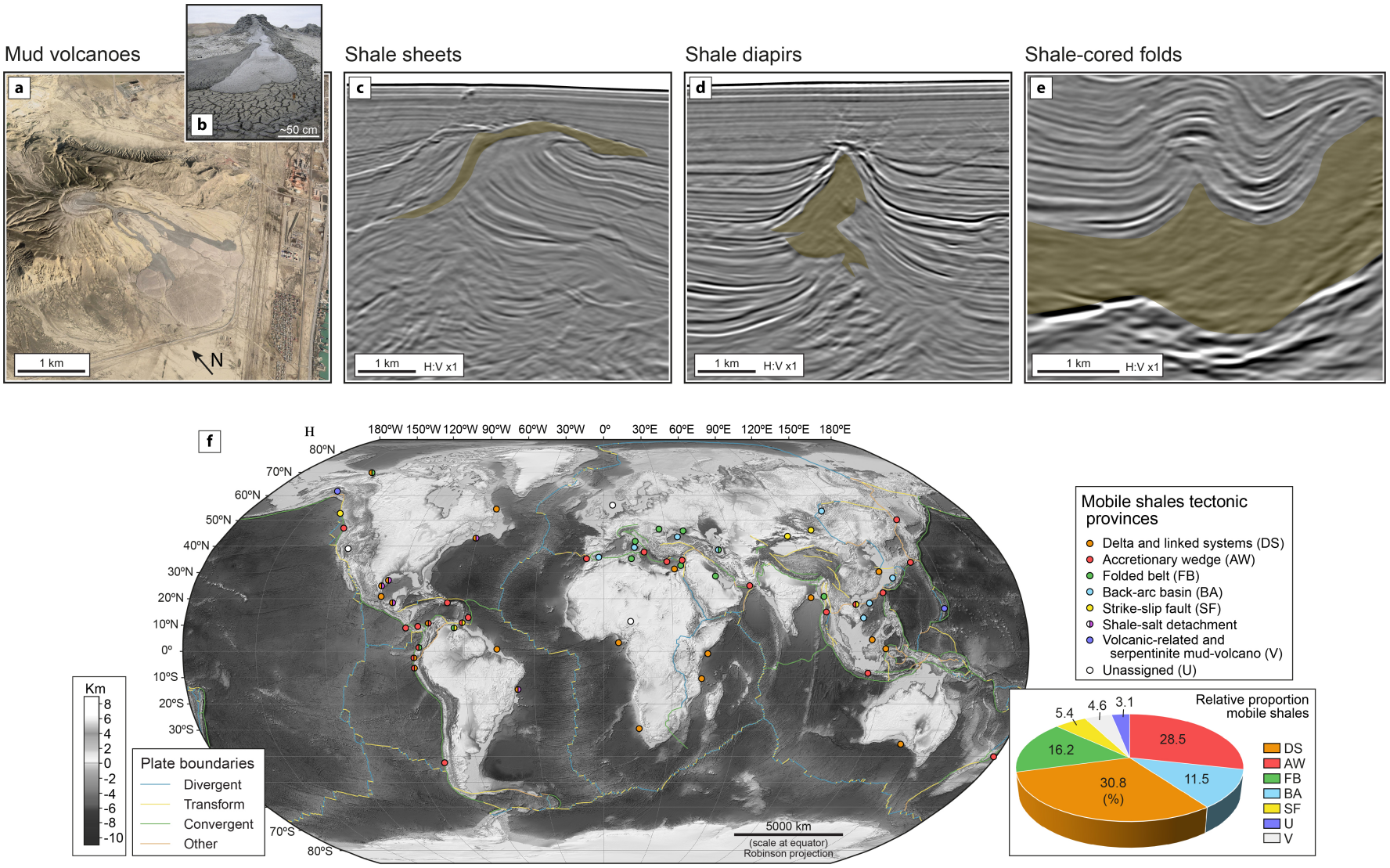

Fig. 1 (legend in next page)

↑ **Fig. 1 | Structures formed by mobile shales. a**, Garadagh mud volcano in onshore Azerbaijan (40.24°N and 49.51°E). **b**, Gryphon structure within the Dashgil mud volcano[49] in onshore Azerbaijan (39.99°N and 49.47°E). **c–e**, Buried mobile shales, as seen in seismic profiles (offshore, north-western Gulf of Mexico): **c**, shale sheet; **d**, shale diapir, and **e**, shale-cored folds. Seismic images extracted from a 3D depth seismic cube (seismic data courtesy of PGS). **f**, Global distribution of mobile-shale structures over plate-tectonic map of Earth. Surface-elevation model and complete details of compilation in Supplementary Discussion 1 (Fig. s1 and Table s1). Map plotted using Robinson projection. Inset pie diagram shows relative proportion (in %) of mobile shales according to their tectonic setting (for total population of 65 regions; Supplementary Table s1).

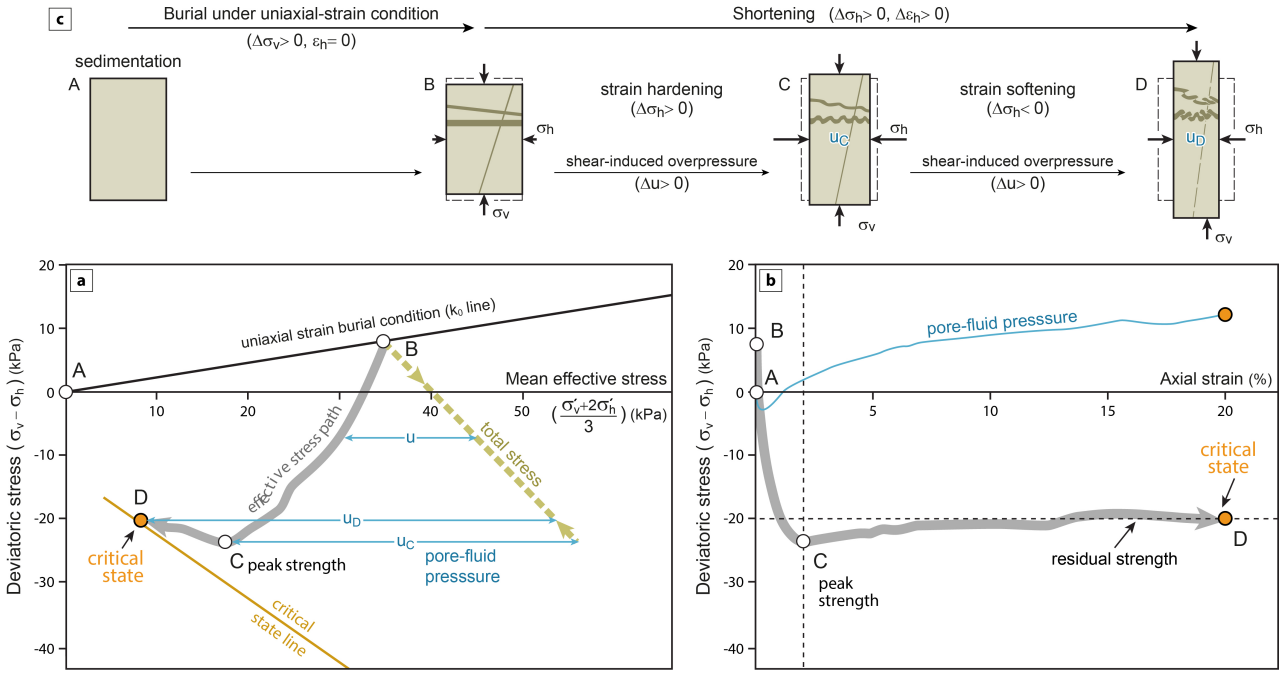

Fig. 2 | Mechanical behaviour of shales. **a**, Stress paths of an anisotropic clay (Norrköping clay) as depicted in the p′-q space (mean effective stress vs. deviatoric stress), according to experimental results of undrained triaxial compression tests[39] (using results with high pre-consolidation stress). **b**, Stress-strain curve of sample (axial strain vs. deviatoric stress) and variation of pore-fluid excess pressure during experiment. **c**, Approximate variation in idealized sample of main stresses and strain during evolution from sedimentation (A) to critical state (D). Note how different passive markers in sample can be deformed and finally disrupted when fabric collapses and rock achieves critical state. A to B: Uniaxial strain consolidation; B to C: undrained shearing deformation, sample exhibiting strain-hardening until peak strength (C); and C to D: undrained-shearing, sample exhibiting strain-softening due to fabric collapse. Additional experiments documenting how shales can achieve critical state conditions in Supplementary Discussion 2 (Fig. s2).

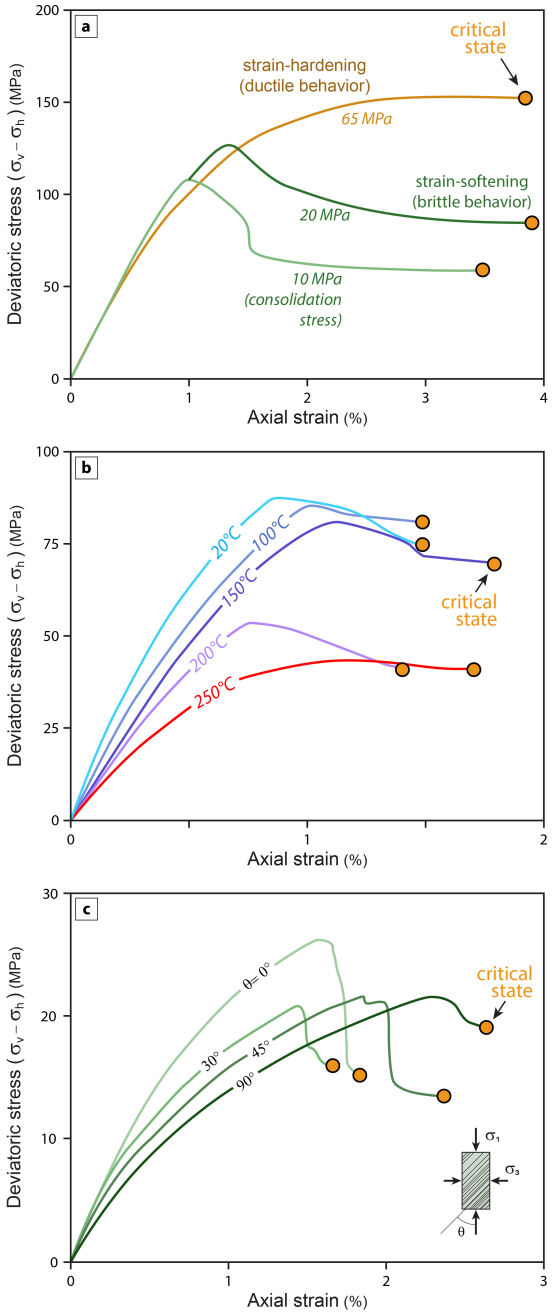

Fig. 3 | Experimental stress-strain curves and critical-state conditions in shales. **a**, Mudstone samples from Kuqa Depression (Tarim Basin, China) deformed at different consolidation stresses[46]. Brittle behaviour characterized by strain-softening (experiments at consolidation stresses of 10 and 20 MPa), ductile behaviour showing no difference between peak and residual strengths (consolidation stress of 65 MPa). Tests with compression perpendicular to bedding. **b**, Stress-strain curves for Tournemire shale (Massif Central, France) deformed at different temperatures[47]. Tests under constant consolidation stress (20 MPa) and compression perpendicular to bedding. **c**, Stress-strain curves for Pierre-1 shale (USA) deformed with different orientations (θ) of bedding[509]. Tests under constant consolidation stress (25 MPa). Other symbols like in Fig. 2. Detailed information about these experimental tests and about shale samples in Supplementary Discussion 2 (Tables s2–s3). Additional experiments documenting how confining pressure, temperature, and fabric anisotropy affect geomechanical behaviour of shales in Figs. s3, s4, and s5, respectively (Supplementary Discussion 2).

Acknowledgements

We thank Nancy Cottington for initial figure drafting. The project was funded by the Applied Geodynamics Laboratory (AGL) Industrial Associates program, comprising the following companies: Anadarko, Aramco Services, BHP Billiton, BP, CGG, Chevron, Condor, Ecopetrol, EMGS, ENI, ExxonMobil, Hess, Ion-GXT, Midland Valley, Murphy, Nexen USA, Noble, Petrobras, Petronas, PGS, Repsol, Rockfield, Shell, Spectrum, Equinor, Stone Energy, TGS, Total, WesternGeco, and Woodside (http://www.beg.utexas.edu/agl/sponsors). Publication authorized by the Director, Bureau of Economic Geology, The University of Texas at Austin.

Author contributions

J.I.S., M.H. and M.R.H. conceived and designed the study, co-writing the paper.

Competing interests

The authors declare no competing interests.

Additional information

Supplementary Discussion 1. Global distribution of mobile-shale structures

Figure s1 (Global distribution of the mobile-shale structures according to tectonic setting)

Table s1 (List of regions with mobile shales)

Supplementary references for Fig. s1

Supplementary Discussion 2. Composition and geomechanical-test conditions in shales

Table s2 (Composition and geomechanical-test conditions of various shales compiled for this study)

Table s3 (Ternary diagrams for classification of shales)

Figure s2 (Stress paths and stress-strain curves for shales—Supplementary to Fig. 2)

Figure s3 (Stress-strain curves for shales under different confining pressures—Supplementary to Fig. 3a)

Figure s4 (Stress-strain curves for shales under different temperature conditions—Supplementary to Fig. 3b)

Figure s5 (Stress-strain curves for shales depending on orientation of fabric—Supplementary to Fig. 3c)

Figure s6 (Shear strength of London Clay measured using Vane test)

Supplementary references for Tables s2−s3 and Figures s2−s6

Supplementary Files

This is a list of supplementary files associated with this preprint. Click to download.

- SupplementaryMaterialSotoetal.pdf